Intelligent Reflecting Surface Aided Wireless Power Transfer with a DC-Combining based Energy Receiver and Practical Waveforms

Qingdong Yue, Jie Hu, *Senior Member, IEEE*, Kun Yang, *Senior Member, IEEE*

***Abstract*—This paper studies intelligent reflecting surface (IRS) aided wireless power transfer (WPT) to batteryless Internet of Everything (IoE) devices. A practical energy receiver (ER) with multiple antennas is investigated. Multiple RF energy flows gleaned by all the receive antennas are input multiple energy harvesters, which are further rectified to direct-current (DC) energy. The resultant multiple DC energy flows are then combined in the DC domain for energy storage. Three classic waveforms, namely deterministic waveform, M-QAM waveform, and Gaussian waveform, are considered for WPT. We maximize the output DC power by jointly designing the active transmit beamformer of the transmitter and the passive reflecting beamformer of the IRS with the above-mentioned waveforms, respectively, subject to the transmit power constraint at the transmitter and to the limited resolution constraints on the phase-shifters of the IRS. A low complexity alternating optimization (AO) algorithm is proposed, which converges to a Karush-Kuhn-Tucker (KKT) point and thus results in a locally optimal solution. The numerical results demonstrate that the Gaussian waveform has the best energy performance with a low input RF power to the energy harvesters. By contrast, the deterministic waveform becomes superior with a high input RF power to the energy harvesters.**

***Index Terms*—Wireless power transfer (WPT), intelligent reflecting surface (IRS), MIMO, practical waveforms, practical energy receiver.**

I. INTRODUCTION

Recently, low-power Internet of Everything (IoE) deveices are massively deployed. Their energy supply normally comes from embedded batteries. However, quickly drained batteries largely limit functions of IoE devices. Fortunately, radio frequency (RF) signals are reliable to transfer wireless power to these devices [1]–[4]. In traditional communications, M-QAM and Gaussian waveforms are exploited to transmit information. However, are these waveforms still suitable for wireless power transfer (WPT)? Furthermore, deterministic waveforms were considered for dedicated WPT. Clerckx *et. al.* [5]–[8] studied a waveform design for the WPT by approximating non-linear energy harvesters with the classic Taylor expansion. However, it is only appropriate within a very small region of the input RF-power. The Taylor expansion based approximation can not accurately characterise RF-direct current (DC) energy conversion with a large range of input RF power. Therefore, we need to carefully design waveforms by considering a more accurate energy harvesting model.

Qingdong Yue, Jie Hu and Kun Yang are with the School of Information and Communication Engineering, University of Electronic Science and Technology of China, Chengdu, 611731, China, email: qdyue1588@163.com, hujie@uestc.edu.cn and kunyang@uestc.edu.cn.

In order to improve WPT performance, the multiple-input-multiple-output (MIMO) technique is invoked for providing spatial gains. Specifically, Zhang *et. al.* [9] designed a predecoder for simultaneous wireless information and power transfer (SWIPT) in a MIMO aided broadcast system to maximize the achievable rate, while satisfying the energy requirements and transmit power budget. Zhong *et. al.* [10] studied WPT in the beamspace of a large-scale MIMO system to maximize the receive RF power by optimizing the transmit beamformer. Most of MIMO-SWIPT or MIMO-WPT related works [11]–[15] presumed that the total RF power was the sum of the RF power gleaned by every receive antenna. The resultant total RF power input to an energy harvester for being rectified to the DC power. However, this is impractical in terms of hardware implementation. This is because the energy stream of every antenna is alternating current with different phases. They are not always constructively combined without any intervention. Therefore, how to deal with the multiple energy flows gleaned by multiple antennas of an energy receiver is still an open problem.

Intelligent reflecting surface (IRS) composed of a large number of low-cost reflecting elements is regarded as a key enabling technique for future 6G [16]–[18]. An IRS is capable of passively reflecting incident RF signals by adjusting their phases in the analog domain [19]–[21]. The passive beams can be adjusted to accurately aim at receivers to improve the wireless communication performance, due to the large spatial gain provided by the IRS. The IRS does not invoke any active power-consuming RF chains, which substantially reduces its hardware complexity and energy-consumption. Furthermore, line-of-sight (LoS) is beneficial for both the WPT and the SWIPT in order to counteract severe fading of wireless channels. When the channel from the transmitter to the receiver is non-LoS, the IRS is capable of creating an LoS alternative from the transmitter to the receiver via the IRS [22], [23]. Therefore, the IRS can substantially increase the WPT performance.

Specifically, Wu *et. al.* [24] designed transmit precoders and reflecting phase-shifters at all IRSs in a SWIPT system to minimize the transmit power at the AP, subject to quality-of-service (QoS) constraints at both information users and energy users, respectively. Faissal *et. al.* [25] explored the outage probability and average symbol error probability for the IRS aided wireless networks with SWIPT. Yuan *et. al.* [26] studied an IRS-assisted wireless powered communication network, where two users harvested wirelss energy and transmitted

information to a common hybrid access point. Pan *et. al.* [27] considered an IRS-assisted SWIPT system, where the transmitter communicated with the information users, while satisfying the energy requirements of energy users. Zou *et. al.* [28] studied a batteryless IRS, which is capable of IRS harvesting energy and reflecting signal. They designed the transmit beamformer, the IRS's time allocation and passive reflecting beamformer to maximize the achievable rate. Lyu *et. al.* [29] studied a wireless powered IRS. They conceived both the time-switching and power-splitting schemes for the IRS, which could adaptively switch between the energy harvesting mode and the signal reflection mode. Niu *et. al.* [30] studied the IRS aided MIMO secure SWIPT system. They aimed to maximize the secrecy rate by optimizing the transmit precoder, the artificial noise and the phase-shifters of the IRS, subject to various energy requirements. Wu *et. al.* [31] deployed an IRS to assist a access point with multiple antennas. They designed the transmit precoder and passive reflect beamformer to maximize the weighted sum-power received, while satisfying the individual signal-to-interference-plus-noise ratio.

However, the existing works still have following drawbacks

- Most of works are focused on design the transmit precoder and passive beamformer ,while the ER is usually equipped with a single antenna. The multi-antenna aided practical ERs were never considered. The potential spatial gain provided by multiple receive antenna is ignored.
- The conventional WPT waveform design is only appropriate within a very small region of the input RF-power. The Taylor expansion based energy harvester approximation can not accurately characterise RF-DC energy conversion with a large range of input RF power.

Against this background, our novel contributions are summarize as follows:

- The IRS aided MIMO-WPT system is investigated. We propose a practical architecture of the multi-antenna aided ER, where every antenna connects to an energy harvester for rectifying the RF power to DC. Then, the DC flows converted by all the energy harvesters are combined.
- Three waveforms, namely deterministic waveform, M-QAM waveform, and Gaussian waveform are considerred for dedicated WPT. The practical non-linear energy harvesting model is adopted. The output DC power is maximized by jointly designing the active transmit beamformer of the transmitter and the passive reflecting beamformer of the IRS associated with different waveforms, while satisfying the transmit power constraint and the limited resolution constraints on the phase-shifters of the IRS.
- A low complexity alternating optimization (AO) algorithm is proposed, which converges to a Karush-Kuhn-Tucker (KKT) point. The optimal transmit beamformer is derived in closed-form, when the passive reflecting beamformer is given. By exploiting the minorize maximization (MM) method and Lagrangian duality, the passive reflecting beamformer is derived in closed-form when the transmit beamformer is given.
- Numerical results verify the performance advantage of the IRS-aided WPT system and that of our proposed ER architecture. The Gaussian waveform has the best energy performance with a low input RF power to the energy harvester while the deterministic waveform becomes superior with a high input RF power to the energy harvester.

The rest of the paper is organised as follows. System model is are introduced in Section II, while both the problem formulation and the joint design are detailed in Section III. After presenting pivotal numerical results in Section IV, our paper is finally concluded in Section V.

Notation: $(\cdot)^H$ denotes transpose-conjugate operations. $|\mathbf{A}|$ denotes the determinant of matrix $\mathbf{A}$. $|a|$ and $||\mathbf{a}||_2$ are the magnitude of a scalar a and the norm of a vector $\mathbf{a}$, respectively. $||\mathbf{A}||_F$ denotes the Frobenius norm of a matrix $\mathbf{A}$. $\mathbf{A}(i,j)$ represents the element in the i-th row and the j-th column in $\mathbf{A}$. vec$(\mathbf{A})$ is the vectorization of the diagonal of a mateix $\mathbf{A}$. $diag(\mathbf{a})$ is a diagonal matrix constituted by the vector $\mathbf{a}$

II. SYSTEM MODEL

A. IRS Aided WPT System

The IRS aided WPT system has a single transmitter equipped with $N_t > 1$ antennas, a single energy receiver (ER) equipped with $N_r > 1$ antennas and an IRS equipped with $K > 1$ passive reflectors. The wireless channel from the transmitter to the IRS, that from the IRS to the ER and that from the transmitter to the ER are denoted as $\mathbf{G} \in \mathbb{C}^{N_t \times K}$, $\mathbf{H}_r \in \mathbb{C}^{K \times N_r}$ and $\mathbf{H}_d \in \mathbb{C}^{N_t \times N_r}$, respectively, as illustrated in Fig.1. We conceive a linear antenna array at both the transmitter and ER and a 2-dimension uniform reflector array at the IRS. The IRS is connected to the transmitter and controlled by it. We assume that the direct channel $\mathbf{H}_d$ between the transmitter and the ER follows Rayleigh block fading without a clear line-of-sight (LOS) path. The channel coefficient $\mathbf{H}_d(i,j)$ form the i-the transmit antenna to the j-th receive antenna satisfies $\mathbf{H}_d(i,j) \sim \mathcal{CN}(0,1)$ for $\forall i$ and $\forall j$. For the IRS related channels, i.e., $\mathbf{H}_r$ and $\mathbf{G}$, they both obey Rician block fading. For example, The 2D array channel model [32] $\mathbf{H}_r$ between the transmitter and the IRS is expressed as

$$\mathbf{H}_r = \sqrt{\frac{\beta}{\beta+1}}{\mathbf{H}_r}^{LOS} + \sqrt{\frac{1}{\beta+1}}{\mathbf{H}_r}^{NLOS} \tag{1}$$

where β is the Rician factor, ${\mathbf{H}_r}^{LOS}$ is the deterministic LOS portion and ${\mathbf{H}_r}^{NLOS}$ is the non-LOS (NLOS) portion.

The LOS portion ${\mathbf{H}_r}^{LOS}$ can be further expressed as ${\mathbf{H}_r}^{LOS} = \mathbf{a}_r(\theta_2,\theta_1)^H\mathbf{a}_t(\theta_4,\theta_3)$. Assume that the IRS are equipped with a 2D uniform rectangular array in the xy-plane with M_1 and M_2 elements on the x and y axes, respectively. The arrival steering vector $\mathbf{a}_r(\theta_2,\theta_1)$ of this 2D array is obtained as

$$\mathbf{a}_r(\theta_2,\theta_1) = \mathbf{a}_{az}(\theta_2,\theta_1) \otimes \mathbf{a}_{el}(\theta_2,\theta_1), \tag{2}$$

where θ_2 and θ_1 are the azimuth and elevation angles, respectively, while $\otimes$ represents the Kronecker product. Moreover,

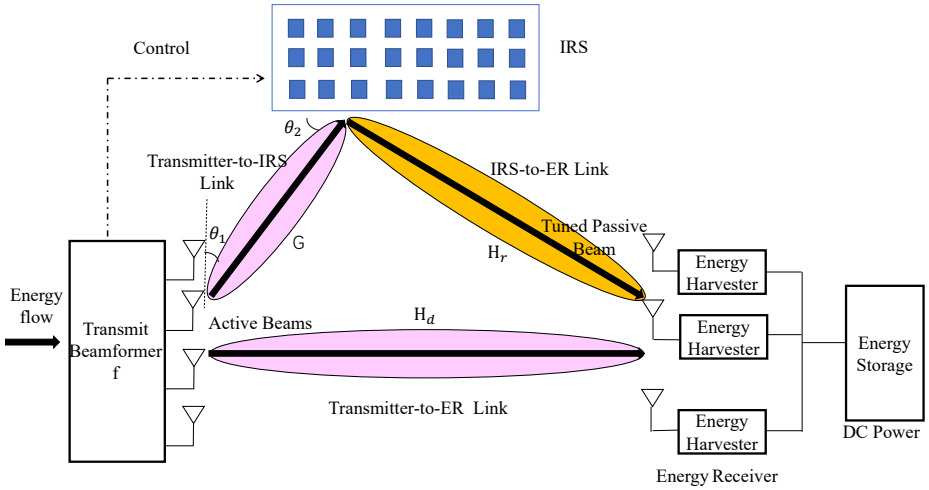

Fig. 1. IRS added MIMO system.

$\mathbf{a}_{az}(\theta_2,\theta_1) \in \mathbb{C}^{M_1\times 1}$ and $\mathbf{a}_{el}(\theta_2,\theta_1) \in \mathbb{C}^{M_2\times 1}$ are the uniform linear array steering vector expressed as

$$[\mathbf{a}_{az}(\theta_2,\theta_1)](n) = e^{-j(n-1)\frac{2\pi}{\lambda}d_1 sin(\theta_2)cos(\theta_1)}, \quad (3)$$

$$[\mathbf{a}_{el}(\theta_2,\theta_1)](n) = e^{-j(n-1)\frac{2\pi}{\lambda}d_1 sin(\theta_2)cos(\theta_1)}, \quad (4)$$

where λ is the wavelength, d_1 is the distance between two adjacent antennas. The departure steering vector $\mathbf{a}_t(\theta_4,\theta_3)$ has the same form as $\mathbf{a}_r(\theta_2,\theta_1)$, where θ_3 and θ_4 represent the azimuth and elevation angles, respectively.

The transmit signal for the dedicated WPT is expressed as $\mathbf{x} = \mathbf{f}s$ where s is an 1×1 complex signal and $\mathbf{f} \in \mathbb{C}^{N_t\times 1}$ is the active transmit beamformer. Let us denote the phase-shifter of the k-th passive reflector of the IRS by $\phi_k \in \mathcal{F}$, where $\mathcal{F} \triangleq \{e^{\frac{j2\pi b}{2^B}} | b = 1,2,\cdots,2^B\}$. The passive reflector simply multiplies the incident multi-path signals by ϕ_k and it then reflects the adjusted signal to the ER. The ER receives the RF signal directly transmitted by the transmitter and that reflected by the IRS, which is then expressed as

$$\mathbf{y} = (\mathbf{H}_d + \mathbf{G}\mathbf{\Phi}\mathbf{H}_r)\mathbf{f}s + \mathbf{n}, \quad (5)$$

where $\mathbf{y} \in \mathbb{C}^{N_r\times 1}$ is the received RF signal, $\mathbf{\Phi} \in \mathbb{C}^{K\times K}$ is the diagonal phase-shifter matrix having $diag(\mathbf{\Phi}) = \{\beta_1\phi_1, \beta_2\phi_2, \cdots, \beta_K\phi_K\}$. Note that $\beta_k \in [0,1]$ is the amplitude reflection coefficient of the k-th passive reflector. We assume that $\beta_k = 1$ for $\forall k$, while $\mathbf{n}$ is the antenna noise satisfying $\mathbf{n} \sim \mathcal{CN}(0,\sigma^2)$. Let us denote the equivalent channel between all the transmit antennas and the receive antennas as $[\mathbf{h}_1,\mathbf{h}_2,\cdots,\mathbf{h}_{N_r}] = \mathbf{H} = \mathbf{H}_d + \mathbf{G}\mathbf{\Phi}\mathbf{H}_r$.

B. Practical Energy Harvester

Boshkovska *et. al.* [33] found that a diode based rectifier is non-linear for rectifying the RF power to the DC one. According to [33], the non-linear rectifying model with a saturation phenomenon is expressed as

$$\Psi(P) = \frac{M}{X(1+\exp(-a(P-b)))} - Y, \quad [Watt] \quad (6)$$

where $X = \frac{\exp(ab)}{1+\exp(ab)}$ and $Y = \frac{M}{\exp(ab)}$, P is the input RF power and $\Psi(P)$ is the output DC power. Moreover, M denotes the saturated upper-bound of the output DC power, while the constants a and b represent the joint impact of the resistances, the capacitances, and the circuit sensitivity on the rectifying process.

The DC-domain energy combining based architecture is illustrated in Fig. 1. Each receive antenna is directly connected to a non-linear energy harvester. The RF power gleaned by every antenna is input to the corresponding energy harvester. Then, the output DC of all the energy harvesters are combined together to be further stored in an energy storage unit.

C. Different Waveforms

When the deterministic sinusoidal waveform is adopted, we have $||s||^2 = 1$. As for the random modulated waveform, we have $\mathbb{E}||s||^2 = 1$. As shown in Fig. 2, the deterministic sinusoidal waveforms have the same amplitudes. By contrast, a random waveform does not carry stable energy. This is because amplitude of the waveform are exploited for modulating different information. As shown in Fig. 2, the 16-QAM based waveform has various amplitudes in different symbol durations. Especially, there are some symbols carried more power than the average power. Furthermore, there are more amplitude variations in the Gaussian waveform.

The discrete baseband signal model is adopted in our paper for WPT. However, the continuous passband signal model is implemented in the practice. Therefore, we have the following proposition.

Proposition 1: The discrete baseband signal model is equivalent to the continuous passband signal model for WPT.

Proof: Please refer Appendix A. ■

Case 1: Deterministic sinusoidal waveform

When the deterministic sinusoidal waveform is adopted for WPT, the received signal of the l-th antenna is expressed as

$$y_l = \mathbf{h}_l\mathbf{f}s + \mathbf{n}, \quad (7)$$

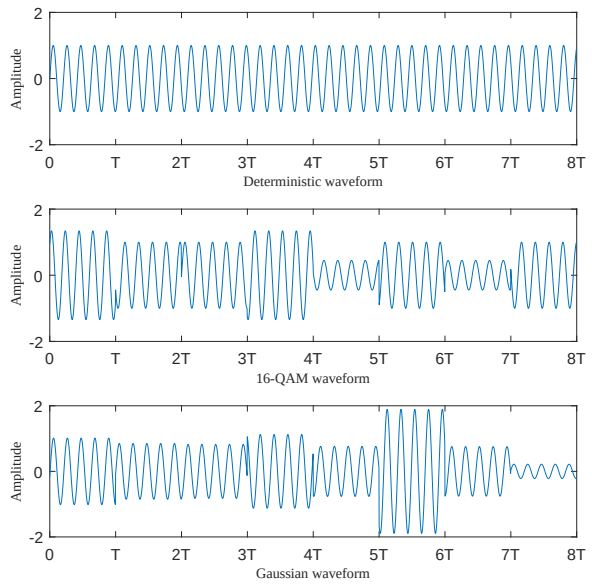

Fig. 2. Amplitudes of three waveforms with the same average power.

where s is the discrete version of deterministic sinusoidal waveform. Therefore, we have $||s||^2 = 1$. The RF power gleaned by the l-th antenna is expressed as

$$P_{RF,l} = ||y_l y_l^H||^2 = ||\mathbf{h}_l \mathbf{f} s||^2 = ||\mathbf{h}_l \mathbf{f}||^2 \tag{8}$$

Therefore, the total output DC power of the deterministic waveform is obtained as

$$P_{DC}^D = \sum_{l=1}^{N_r} \Psi(P_{RF,l}) = \sum_{l=1}^{N_r} \Psi(||\mathbf{h}_l \mathbf{f}||^2). \tag{9}$$

Case 2: M-QAM waveform

The energy carried by M-QAM based waveform varies in different symbol durations, when different modulated symbols are transmitted. Let us denote a specific transmit waveform as a tuple (s_i, p_i, q_i), $for\ \forall i = 1, 2, \cdots, M$, where s_i represents the i-th modulated symbol, p_i represents its power and q_i represents its transmit probability. Therefore, when s_i is transmitted, the corresponding RF power received by the l-th antenna is expressed as

$$P_{RF,l}^Q = ||\mathbf{h}_l \mathbf{f} s_i||^2 = ||\mathbf{h}_l \mathbf{f}||^2 p_i \tag{10}$$

As a result, the average total output DC power is formulated as

$$P_{DC}^Q = \sum_{i=1}^{M} \sum_{l=1}^{N_r} P_{RF,l} q_i = \sum_{i=1}^{M} \sum_{l=1}^{N_r} \Psi(||\mathbf{h}_l \mathbf{f}||^2 p_i) q_i \tag{11}$$

Case 3: Gaussian waveform

Let s represent the complex Gaussian symbol satisfying $s \sim \mathcal{CN}(0, 1)$ with a probability density function of $f(s)$. The received signal of the l-th antenna is expressed as

$$y_l = \mathbf{h}_l \mathbf{f} s + n. \tag{12}$$

Then, the average total output DC power of the Gaussian waveform is obtained as

$$P_{RF}^G = \sum_{l=1}^{N_r} \int_{-\infty}^{\infty} f(s) \Psi(||\mathbf{h}_l \mathbf{f} s||^2) ds \tag{13}$$

III. Joint Design for WPT Transceiver

A. Joint Design with Deterministic Waveform

Our goal is to maximize the output DC power in the DC combining based architecture of the ER in Fig. 1. By conceiving the deterministic waveform. The objective is formulated as

$$\max_{\mathbf{f}, \mathbf{\Phi}} \sum_{i=1}^{N_r} \Psi(||\mathbf{h}_l \mathbf{f}||^2). \tag{14}$$

However, it is challenging to directly deal with the non-linear energy harvesting function $\Psi(\cdot)$ in Eq.(14). With the aid of the first-order Taylor expansion, the objective function can be reformulated as

$$\max_{\mathbf{f}, \mathbf{\Phi}} \sum_{l=1}^{N_r} (y_l y_l^H) + p_0 = ||(\mathbf{H}_d + \mathbf{G}\mathbf{\Phi}\mathbf{H}_r)\mathbf{f}||_2^2 + p_0, \tag{15}$$

where p_0 is the constant in Taylor expansion. The new objective function Eq. (15) indicates that we aim for maximizing the sum of the RF power gleaned by every receive antenna. We design the transmit beamformer $\mathbf{f}$ at the transmitter and passive reflecting beamformer $\mathbf{\Phi}$ at the IRS by considering the power budget of the transmitter and the finite resolution phase-shifter in the IRS. As a result, the optimization problem is formulated as

$$\text{(P1)}: \max_{\mathbf{f}, \mathbf{\Phi}} ||(\mathbf{H}_d + \mathbf{G}\mathbf{\Phi}\mathbf{H}_r)\mathbf{f}||_2^2 + p_0, \tag{16}$$

$$\text{s.t. } ||\mathbf{f}||_2^2 \leq P_t, \tag{16b}$$

$$\mathbf{\Phi}(k,k) \in \mathcal{F},\ k = 1, \cdots, K, \tag{16d}$$

where P_t is the upper-bound constraint on the transmit power and $\mathcal{F}$ is the finite resolution set for the phase-shifters. An AO based iterative algorithm is proposed for solving (P1) for its non-convexity.

With a given $\mathbf{\Phi}$, (P1) is reformulated as

$$\text{(P1.1)}: \max_{\mathbf{f}} \mathbf{f}^H (\mathbf{H}_d + \mathbf{G}\mathbf{\Phi}\mathbf{H}_r)^H (\mathbf{H}_d + \mathbf{G}\mathbf{\Phi}\mathbf{H}_r)\mathbf{f}, \tag{17}$$

$$\text{s.t. } ||\mathbf{f}||_2^2 \leq P_t, \tag{17b}$$

The eigenvalue decomposition of $(\mathbf{H}_d + \mathbf{G}\mathbf{\Phi}\mathbf{H}_r)^H (\mathbf{H}_d + \mathbf{G}\mathbf{\Phi}\mathbf{H}_r)$ is expressed as $(\mathbf{H}_d + \mathbf{G}\mathbf{\Phi}\mathbf{H}_r)^H (\mathbf{H}_d + \mathbf{G}\mathbf{\Phi}\mathbf{H}_r) = \mathbf{U}^H \mathbf{\Sigma} \mathbf{U}$. The optimal solution to (P1.1) is then obtained in closed form as

$$\mathbf{f} = \sqrt{P_t}\mathbf{u}, \tag{18}$$

where $\mathbf{u}$ is the eigenvector corresponding to the largest eigenvalue of $(\mathbf{H}_d + \mathbf{G}\mathbf{\Phi}\mathbf{H}_r)^H (\mathbf{H}_d + \mathbf{G}\mathbf{\Phi}\mathbf{H}_r)$.

Given a fixed transmit beamformer $\mathbf{f}$, (P1) is reformulated as

$$\text{(P1.2)}: \max_{\mathbf{\Phi}} ||(\mathbf{H}_d + \mathbf{G}\mathbf{\Phi}\mathbf{H}_r)\mathbf{f}||_2^2 + a, \tag{19}$$

$$\text{s.t. } \mathbf{\Phi}(k,k) \in \mathcal{F}.\ k = 1, \cdots, K, \tag{19d}$$

By relaxing the discrete phase-shifters constrains to the continuous constrains, (P1.2) is convert to

$$\text{(P1.3)}: \max_{\mathbf{\Phi}_c} ||(\mathbf{H}_d + \mathbf{G}\mathbf{\Phi}_c\mathbf{H}_r)\mathbf{f}||_2^2 + a, \tag{20}$$

$$\text{s.t. } ||\mathbf{\Phi}_c(k,k)|| = 1.\ k = 1, \cdots, K, \tag{20d}$$

where $\mathbf{\Phi}_c$ denotes the continuous phase-shifters in the IRS.

The minorize-maximization (MM) technique can be invoked for solving (P1.3). By adopting $\mathbf{G}\mathbf{\Phi}_c\mathbf{H}_r\mathbf{f} = \mathbf{G}\text{diag}(\mathbf{H}_r\mathbf{f})\text{vec}(\mathbf{\Phi}_c)$ and $\mathbf{\Upsilon} = \mathbf{G}\text{diag}(\mathbf{H}_r\mathbf{f})$, an auxiliary function is defined as

$$F(\text{vec}(\mathbf{\Phi}_c)|\text{vec}(\mathbf{\Phi}_c{}^{[n-1]})) = \tag{21}$$
$$\text{Re}\{\text{vec}(\mathbf{\Phi}_c{}^{[n-1]})\mathbf{\Upsilon}\mathbf{\Upsilon}^H\text{vec}(\mathbf{\Phi}_c)^H + 2\mathbf{f}^H\mathbf{H}_d^H\mathbf{\Upsilon}^H\text{vec}(\mathbf{\Phi}_c)^H\},$$

where $\text{vec}(\mathbf{\Phi}_c{}^{[n-1]})$ is the solution obtained in the $(n-1)$-th iteration. Therefore, a new optimization problem is then formulated as

$$\text{(P1.4)}: \max_{\mathbf{\Phi}_c} F(\text{vec}(\mathbf{\Phi}_c)|\text{vec}(\mathbf{\Phi}_c{}^{[n-1]})), \tag{22}$$

$$\text{s.t. } ||\text{vec}(\mathbf{\Phi}_c)(k)||^2 = 1,\ k = 1, \cdots, K. \tag{22a}$$

Let us denote the optimal solution to (P1.4) as $\text{vec}(\mathbf{\Phi}_c{}^n)$. The following inequality can be satisfied

$$F(\text{vec}(\mathbf{\Phi}_c{}^{[n]})|\text{vec}(\mathbf{\Phi}_c{}^{[n]})) \geq F(\text{vec}(\mathbf{\Phi}_c{}^{[n]})|\text{vec}(\mathbf{\Phi}_c{}^{[n-1]})) \tag{23}$$
$$\geq F(\text{vec}(\mathbf{\Phi}_c{}^{[n-1]})|\text{vec}(\mathbf{\Phi}_c{}^{[n-1]})).$$

The derivation details of Eq. (23) is provided in Appendix B. Therefore, we may achieve a local optimum of (P1.3).

However, (P1.4) is still non-convex because of the unity constrains (22a) on $\mathbf{\Phi}_c{}^n$. By relaxing these unity constraints, the following convex optimization problem is obtained as

$$\text{(P1.5)}: \max_{\mathbf{\Phi}_c{}^{[n]}} F(\text{vec}(\mathbf{\Phi}_c)|\text{vec}(\mathbf{\Phi}_c{}^{[n-1]})), \tag{24}$$

$$\text{s.t. } ||\text{vec}(\mathbf{\Phi}_c{}^{[n]})(k)||^2 \leq 1\ k = 1, \cdots, K. \tag{24a}$$

Proposition 2: The optimal solution to (P1.5) is exactly the same as that to (P1.4).

Proof: Please refer to Appendix C. ∎

Since (P1.5) is convex, the gap between the (P1.5) and its Lagrangian dual counterpart is zero. Therefore, the optimal solution can be obtained by solving the Lagrangian dual problem. The Lagrangian function of (P1.5) is expressed as

$$L(\text{vec}(\mathbf{\Phi}_c{}^{[n]}), \boldsymbol{\lambda}) = \text{Re}\{(\text{vec}(\mathbf{\Phi}_c{}^{[n-1]}))\mathbf{\Upsilon}\mathbf{\Upsilon}^H\text{vec}(\mathbf{\Phi}_c{}^{[n]})^H \tag{25}$$
$$+ 2\mathbf{f}^H\mathbf{H}_d^H\mathbf{\Upsilon}^H(\text{vec}\mathbf{\Phi}_c{}^{[n]})^H\}$$
$$+ \sum_{k=1}^{K} \boldsymbol{\lambda}_m(\text{vec}(\mathbf{\Phi}_c{}^{[n]})(k)(\text{vec}(\mathbf{\Phi}_c{}^{[n]})(k))^H - 1).$$

The Lagrangian dual function can be obtained by solving the following problem

$$g(\boldsymbol{\lambda}) \triangleq \max_{\text{vec}(\mathbf{\Phi}_c^{[n]})} L(\text{vec}(\mathbf{\Phi}_c{}^n), \boldsymbol{\lambda}). \tag{26}$$

Then, the Lagrangian dual problem is formulated as

$$\text{(P1.6)}: \max_{\boldsymbol{\lambda}} g(\boldsymbol{\lambda}), \tag{27}$$

$$\text{s.t. } \boldsymbol{\lambda}(k) \geq 0\ k = 1, 2, \cdots, K. \tag{27a}$$

The KKT conditions on (P1.6) is obtained as

$$\begin{cases} \boldsymbol{\lambda}(k) \geq 0,\ k = 1, 2, \cdots, K, \\ \boldsymbol{\lambda}(k)(\text{vec}(\mathbf{\Phi}_c{}^{[n]})(k)(\text{vec}(\mathbf{\Phi}_c{}^{[n]})(k))^H - 1) = 0, \\ \quad k = 1, 2, \cdots, K, \\ \mathbf{a}(k) + \mathbf{b}(k) + \boldsymbol{\lambda}(k)\text{vec}(\mathbf{\Phi}_c)^{[n]}(k) = 0, \\ \quad k = 1, 2, \cdots, K, \end{cases} \tag{28}$$

where $\mathbf{a} = (\text{vec}(\mathbf{\Phi}_c{}^{[n-1]}))\mathbf{\Upsilon}\mathbf{\Upsilon}^H$ and $\mathbf{b} = 2\mathbf{f}^H\mathbf{H}_d^H\mathbf{\Upsilon}^H$. By solving Eq.(28), the m-th element in $\text{vec}(\mathbf{\Phi}_c{}^{[n]})$ is expressed in close-form as

$$\text{vec}(\mathbf{\Phi}_c{}^{[n]})(k) = (\mathbf{a}(k) + \mathbf{b}(k))^H/||\mathbf{a}(k) + \mathbf{b}(k)|| \tag{29}$$

Given a fixed $\text{vec}(\mathbf{\Phi}_c{}^{[n-1]})$, we can obtain $\text{vec}(\mathbf{\Phi}_c{}^{[n]})$ with the aid of Eq. (29). As a result, by initialising $\text{vec}(\mathbf{\Phi}_c{}^0)$, we may sequentially obtain $\text{vec}(\mathbf{\Phi}_c{}^{[0]})$, $\text{vec}(\mathbf{\Phi}_c{}^{[1]})$, $\cdots$, $\text{vec}(\mathbf{\Phi}_c{}^{[n]}), \cdots$. Since both the objective function and the constraints are continuous, and the constraints indicate closed intervals according to Eq. (22a), the optimum has a upper bound. When n is sufficiently large, the objective of (P1.5) eventually converges. The corresponding $\text{vec}(\mathbf{\Phi}_c{}^*) = \text{vec}(\mathbf{\Phi}_c{}^{[n]})$ can be regarded as the local optimal solution to (P1.3). Therefore, We may obtain the continuous passive reflecting beamformer $\mathbf{\Phi}_c$ of the IRS.

The transmit beamformer $\mathbf{f}$ is obtained by (P1.1) with fixed $\mathbf{\Phi}$. And the passive reflecting beamformer $\mathbf{\Phi}$ is obtained by (P1.5) with given $\mathbf{f}$. An alternating optimization algorithm is proposed. According to Eq.(28), the local optimal $\mathbf{\Phi}_c{}^{[n]}$ satisfies the KKT condition. Since the transmit beamformer $\mathbf{f}$ is the optimal solution, it also satisfies the KKT condition. Therefore, our algorithm converges to a KKT point.

The discrete phase-shifters of the IRS solution can be obtained as

$$\mathbf{\Phi}^*(k) = \arg\min_{\mathbf{\Phi}(k,k)} ||\mathbf{\Phi}(k) - \mathbf{\Phi}_c^*(k,k)||, \tag{30}$$

which can be solved by a one-dimension exhaustive search. The main steps for solving (P1) is summarised in Algorithm 1. The complexity of Algorithm 1 is $O(M^3 I_{inner} I_{outer})$, where I_{inner} and I_{outer} the number of inner and outer iteration, respectively.

B. M-QAM Waveform Design

When the M-QAM waveform is adopted at the transmitter, the objective function is formulated as

$$\max_{\mathbf{f},\mathbf{\Phi}} \sum_{i=1}^{M} \sum_{l=1}^{N_r} \Psi(||\mathbf{h}_l\mathbf{f}||^2 p_i) q_i. \tag{31}$$

Algorithm 1 Joint Transmit Beamformer and Passive Reflect Beamformer Design

Input: The channel $\mathbf{H}_d$, $\mathbf{H}_r$ and $\mathbf{G}$. Initialize the transmit beamformer $\mathbf{f}$, energy combiner $\mathbf{w}$ and the passive reflecting beamformer $\text{vec}(\mathbf{\Phi}_c{}^{[0]})$ of the IRS; error tolerance ε; $F^1 = P^1 = 0$; $n = 0$;

Output: The phase-shifter $\text{vec}(\mathbf{\Phi}_c)^*$ of the IRS;

while $(\Delta > \varepsilon)$ **do**
  Update $P^0 \leftarrow P^1$;
  while $(\delta > \varepsilon)$ **do**
    Update $n \leftarrow n + 1$;
    Update $F^0 \leftarrow F^1$;
    Obtain the the phase-shifters $\text{vec}(\mathbf{\Phi}_c{}^n)$ of the IRS by substituting $\text{vec}(\mathbf{\Phi}_c{}^{n-1})$ into Eq. (29);
    Update $F^1 \leftarrow F(\text{vec}(\mathbf{\Phi}_c{}^n)|\text{vec}(\mathbf{\Phi}_c{}^{n-1}))$;
    Update $\delta \leftarrow ||F^1 - F^0||$;
  end while
  Obtain the beamformer $\mathbf{f}^*$ by Eq.(18);
  Update $P^1 \leftarrow |(\mathbf{H}_d + \mathbf{G}\mathbf{\Phi}_c\mathbf{H}_r)\mathbf{f}||_2^2$;
  Update $\Delta \leftarrow ||P^1 - P^0||$;
end while
Obtain the discrete phase of IRS $\mathbf{\Phi}^*$ by Eq. (30);
return $\{\mathbf{f}^*$ and $\mathbf{\Phi}^*\}$.

The first-order Taylor expansion of Eq. (31) is then obtained as

$$\begin{aligned}&\max \sum_{i=1}^{M}\sum_{l=1}^{N_r}\Psi(||\mathbf{h}_l\mathbf{f}||^2 p_i)q_i \qquad (32)\\ &\approx \max \sum_{i=1}^{M}[||(\mathbf{H}_d + \mathbf{G}\mathbf{\Phi}\mathbf{H}_r)\mathbf{f}||^2 p_i q_i + p_0 q_i\\ &= \max ||(\mathbf{H}_d + \mathbf{G}\mathbf{\Phi}\mathbf{H}_r)\mathbf{f}||^2 + p_0\end{aligned}$$

By adopting the M-QAM waveform, the optimization problem is then formulated as

$$\text{(P2)}: \max_{\mathbf{f},\mathbf{\Phi}} ||(\mathbf{H}_d + \mathbf{G}\mathbf{\Phi}\mathbf{H}_r)\mathbf{f}||_2^2 + p_0, \qquad (33)$$

$$\text{s.t. } (16b), (16d). \qquad (34)$$

Since (P2) has a similar form as (P1), it can also be solved by Algorithm 1.

C. Gaussian Waveform Design

As for the Gaussian waveform, the optimization problem can be formulated as

$$\text{(P3)}: \max_{\mathbf{f},\mathbf{\Phi}} 2\sum_{i=1}^{Nr}\int_0^{\infty} f(s)\Psi(||\mathbf{h}_l\mathbf{f}s||^2)ds, \qquad (35)$$

$$\text{s.t. } (16b), (16d). \qquad (36)$$

The integral $\int_{-\infty}^{\infty} f(s)\Psi(||\mathbf{h}_l\mathbf{f}s||^2)ds$ in the objective function (35) can not be expressed in closed-form. According to the basic definition of integration, this integral can be reformulated as

$$\begin{aligned}&\int_0^{\infty} 2f(s)\Psi(||\mathbf{h}_l\mathbf{f}s||^2)ds \qquad (37)\\ &= 2\lim_{k\to+\infty}\sum_{i=0}^{k}\frac{f[(2i+1)/k]}{k}\Psi(||\mathbf{h}_l\mathbf{f}(2i+1)/k||^2\end{aligned}$$

where $\lim_{k\to+\infty}\sum_{i=0}^{k} 2f[(2i+1)/k]/k = 1$. Eq.(37) indicates that when k is sufficiently large, the average of a continuous random variable s can be approximated by that of a discrete random variable. Therefore, the optimization for Gaussian waveform is equivalent to the M-QAM waveform.

IV. Numerical Results

The transmitter is equipped with $N_t = 4$ antennas, while the energy receiver is equipped with $N_r = 3$ antennas. The number of reflectors in the IRS is $M = 200$. The distances from the transmitter to the IRS and that to the ER are 1 m and 5.5 m, respectively, while the distance form the IRS to the ER is 5m. The path loss is modelled in dB as $PL = PL_0 - 10\alpha\log(d/d_0)$, where PL_0 is the path loss at the reference distance d_0, d is the signal propagation distance and α represents the path loss exponent. We set PL_0 to -30 dB when $d_0 = 1$ m. The pass-loss exponent of the transmitter-IRS-ER link and the transmitter-ER link are set to $\alpha = 2.2$ and $\alpha = 3.6$ [27], respectively. The transmit antenna gain is set to 15 dBi. For the non-linear energy harvesting model of Eq. (6), we set $M = 24$ mW as the maximum DC power that could be output by a single energy harvester. Moreover, we set $a = 150$ and $b = 0.0022$ [34]. The resolution of phase-shifter in IRS is set to 2 Bit. These parameters are not changed, except particularly mentioned.

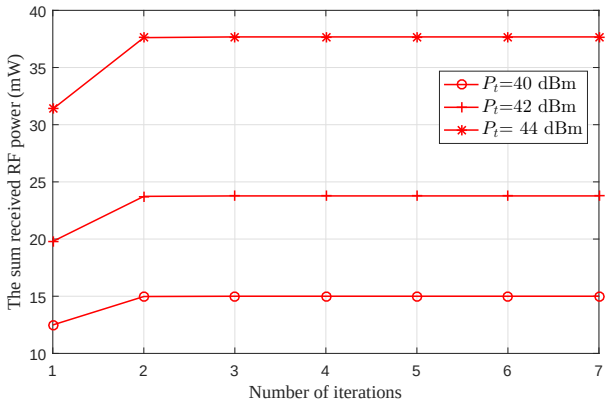

Fig. 3. Iteration vs output power when $N_t = 4$,$N_r = 3$,$M = 200$.

We demonstrate the convergence of the proposed Algorithm 1 in Fig. 3. As shown in Fig. 3, our algorithm converges pretty fast. With different transmit power, the algorithm converges within three or four iterations. Fig.4 illustrates the WPT performances of different waveforms. Observe from Fig. 4 that the 4-QAM waveform has the same WPT performance as the deterministic waveform. This is because 4-QAM based waveform has a stable envelope. When the transmit power is low, the WPT performance of the 16-QAM based waveform is higher than that of the deterministic waveform. This is because some modulated symbols may result in the waveforms carrying more energy than the average. As a result, the non-linear energy harvester can be activated to operate with a high RF-DC energy conversion efficiency, when compared to the deterministic sinusoidal waveform. Furthermore, the Gaussian waveform and the 64-QAM based waveform transfer more

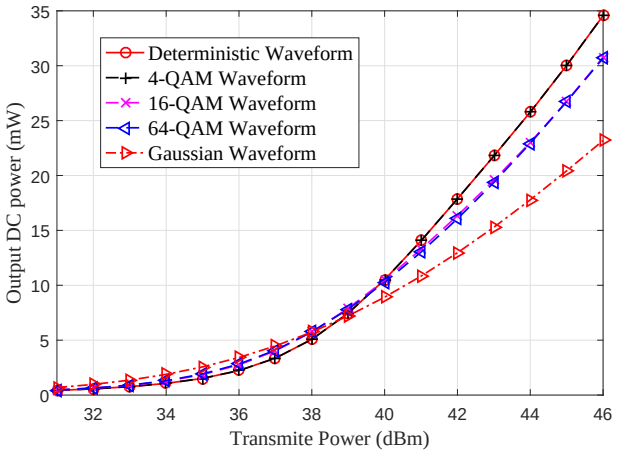

Fig. 4. Transmit power vs output power when $N_t = 4$,$N_r = 3$,$M = 200$.

energy than the 16-QAM based waveform in low transmit power. When the transmit power is high, the deterministic sinusoidal waveform achieves a better WPT performance than the modulated waveform. This is because some modulated symbols result in the waveforms carrying low energy. The non-linear energy harvester has to operate with a low RF-DC conversion efficiency. By contrast, the deterministic sinusoidal waveform can keep the energy harvesters working with a high RF-DC conversion efficiency.

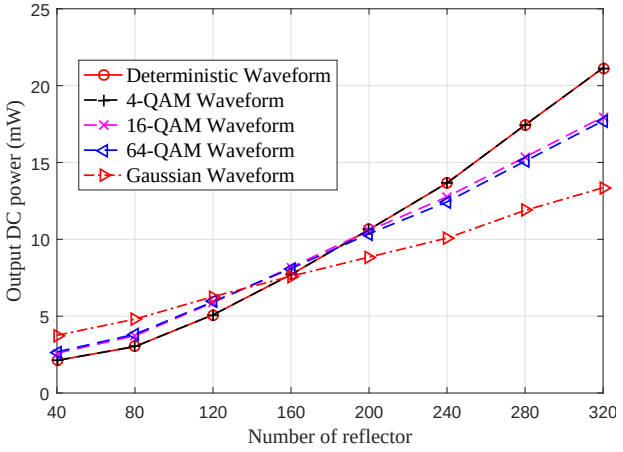

Fig. 5. Number of reflect source vs output power when $N_t = 4$,$N_r = 3$,$P_t = 40dBm$.

We investigate the impact of the number of the reflector in the IRS on the output DC power in Fig. 5, when the transmit power is set to 40 dBm. Observe from Fig. 5 that the output DC power increases as the IRS has more reflectors, since it may provide higher spatial gain for WPT. When the number of reflector is 40, the Gaussian waveform performs the best. When the number of reflector is more than 200, the deterministic sinusoidal waveform has the best WPT performance. This is because the spatial gain increases, since we have more reflectors to be adjusted. Therefore, the deterministic sinusoidal waveform may keep the energy harvesters working with a high RF-DC conversion efficiency by benefiting from this large spatial gain.

V. Conclusion

In the study of an IRS aided MIMO WPT system, we propose a practical multi-antenna aided energy receiver with the DC combining. Three waveforms including deterministic waveform, M-QAM waveform, and Gaussian waveform are considerred for the dedicated WPT. We maximize the output DC power by jointly designing the transmit beamformer of the transmitter and the passive reflecting beamformer of the IRS with different waveforms, subject to the transmit power budget and to the limited resolution constraints on the phase-shifters of the IRS. A low complexity alternating optimization (AO) algorithm is proposed, which is capable of returning a local optimal solution. The numerical results demonstrate that the Gaussian waveform achieves the best WPT performance when the transmit power is low or when the IRS has fewer reflectors. By contrast, when the transmit power is high, the deterministic sinusoidal waveform achieves a best WPT performance than the modulated waveform.

Appendix A
Proof of Proposition 1

Denote $x_{\mathrm{rf},j}(t)$ as the actual transmitted WPT signal on the j-th antenna, which is expressed

$$x_{\mathrm{rf},j}(t) = \sqrt{2}\Re\{x_j(t)e^{i2\pi ft}\}. \tag{38}$$

where $x_j(t)$ is the baseband equivalent signal.

The transmit WPT signal propagates via G different transmission paths. Let τ_g and α_g denote the delay and amplitude profiles of the g-th path, respectively. Moreover, the phase-shift of the g-th transmission path between the transmit antenna j and the receive antenna l is denoted as $\zeta_{l,j,g}$. We normally assume that $x_j(t)$ is a narrowband signals. Therefore, we have $x_j(t-\tau_g) = x_j(t)$, for $\forall g = 1, 2, \cdots, G$. Moreover, the baseband channel response between the transmit antenna j and receive antenna l with a carrier frequency of f is denoted as $h_{l,j} = \sum_{g=1}^{G} \alpha_g e^{i(-2\pi f\tau_g + \zeta_{l,j,g})}$.

As a result, the signal received at the receive antenna l ($l = 1, \cdots, N_r$) from the transmit antenna j can be expressed as

$$\begin{aligned} y_{\mathrm{rf},l,j}(t) =& \sqrt{2}\Re\left\{\sum_{g=1}^{G} \alpha_g x_j(t-\tau_g) \times e^{i2\pi f(t-\tau_g)+\zeta_{l,j,G}}\right\}, \\ =& \sqrt{2}\Re\left\{h_{l,j}x_j(t)e^{i2\pi f_n t}\right\}, \end{aligned} \tag{39}$$

for $\forall l = 1, \cdots, N_r$ and $\forall j = 1, \cdots, N_t$. Moreover, the total signal received by the receive antenna i is expressed as

$$y_{\mathrm{rf},l}(t) = \sqrt{2}\Re\left\{\mathbf{h}_l\mathbf{x}(t)e^{i2\pi ft}\right\} + w_{\mathrm{A},l}(t), \tag{40}$$

where $w_{A,l}(t)$ is the antenna noise, $\mathbf{h}_l = [h_{l,1}, \cdots, h_{l,N_t}]$ denotes the channel response vector from the N_t transmit antennas to the receive antenna i and $\mathbf{x}(t) = [x_1(t), \cdots, x_{N_t}(t)]^T$ represents the signals transmitted by the N_t antennas. The baseband received signal is then expressed as

$$y_l(t) = \mathbf{h}_l\mathbf{x}(t) + w_l(t), \tag{41}$$

where $w_l(t)$ is the received filtered noise, accounting for both the antenna and the RF-to-baseband processing noise. Note that the energy of a passband signal is equal to its baseband version. The only difference is their carrier frequency. Therefore, this does not affect our calculation on the wireless power transfer performance. The discrete complex baseband signal is equivalence to the continuous real passband signal when dealing with wireless power transfer. We have discussed the equivalence between passband signals and their continuous baseband versions. Due to the assumption that the channel stays constant during the coherence time, we can drop the time index t, which is expressed as

$$y_l = \mathbf{h}_l \mathbf{x} + w_l. \tag{42}$$

After stacking the observations from all receive antennas, we obtain

$$\mathbf{y} = \mathbf{H}\mathbf{x} + \mathbf{w}. \tag{43}$$

Therefore, discrete complex baseband signals are equivalent to continuous real passband signals.

Appendix B
Proof of Equation (20)

We first consider the inequality of $F(\text{vec}(\mathbf{\Phi}_c{}^n)|\text{vec}(\mathbf{\Phi}_c{}^{n-1})) \geq F(\text{vec}(\mathbf{\Phi}_c{}^{n-1})|\text{vec}(\mathbf{\Phi}_c{}^{n-1}))$. The function $F(\text{vec}(\mathbf{\Phi}_c)^n|\text{vec}(\mathbf{\Phi}_c{}^{n-1}))$ can be expressed as

$$\begin{aligned} &F(\text{vec}(\mathbf{\Phi}_c)^n|\text{vec}(\mathbf{\Phi}_c{}^{n-1})) = \text{Re}\{\text{vec}(\mathbf{\Phi}_c{}^{n-1})\mathbf{\Theta}\mathbf{\Theta}^H \\ &\times \text{vec}(\mathbf{\Phi}_c^n)^H + 2\mathbf{w}_c^H \mathbf{H}_d \mathbf{\Theta}^H \text{vec}(\mathbf{\Phi}_c^n)^H\}. \end{aligned} \tag{44}$$

We then obtain $\mathbf{\Phi}_c^n$ by solving the following optimization problem:

$$\text{(P1.3):} \max_{\mathbf{\Phi}_c^n} F(\text{vec}(\mathbf{\Phi}_c^n)|\text{vec}(\mathbf{\Phi}_c{}^{n-1})), \tag{45}$$

$$\text{s.t. } ||\text{vec}(\mathbf{\Phi}_c^n)(k)||^2 = 1 \ k = 1, \cdots, K. \tag{45a}$$

Note that $\mathbf{\Phi}_c^{n-1}$ is a feasible solution to (P1.3), while $\mathbf{\Phi}_c^n$ is the optimal one. Therefore, we obtain the inequality of $F(\text{vec}(\mathbf{\Phi}_c{}^n)|\text{vec}(\mathbf{\Phi}_c{}^{n-1})) \geq F(\text{vec}(\mathbf{\Phi}_c{}^{n-1})|\text{vec}(\mathbf{\Phi}_c{}^{n-1}))$.

Next we consider the inequality $F(\text{vec}(\mathbf{\Phi}_c{}^n)|\text{vec}(\mathbf{\Phi}_c{}^n)) \geq F(\text{vec}(\mathbf{\Phi}_c{}^n)|\text{vec}(\mathbf{\Phi}_c{}^{n-1}))$. We have

$$\begin{aligned} &F(\text{vec}(\mathbf{\Phi}_c{}^n)|\text{vec}(\mathbf{\Phi}_c{}^n)) - F(\text{vec}(\mathbf{\Phi}_c{}^n)|\text{vec}(\mathbf{\Phi}_c{}^{n-1})) \\ &= \text{Re}\{\text{vec}(\mathbf{\Phi}_c{}^n)\mathbf{\Theta}\mathbf{\Theta}^H \text{vec}(\mathbf{\Phi}_c^n)^H\} \\ &- \text{Re}\{\text{vec}(\mathbf{\Phi}_c{}^{n-1})\mathbf{\Theta}\mathbf{\Theta}^H \text{vec}(\mathbf{\Phi}_c^n)^H\}. \end{aligned} \tag{46}$$

Observe from this equation that $\mathbf{\Theta}^H \text{vec}(\mathbf{\Phi}_c^n)^H$ is a complex number, while both $\mathbf{\Phi}_c^{n-1}$ and $\mathbf{\Phi}_c^n$ have the same norms. Therefore, the value of the conjugate transpose of $\mathbf{\Phi}_c^n$ is larger than that of $\mathbf{\Phi}_c^{n-1}$. As a result, we have $F(\text{vec}(\mathbf{\Phi}_c{}^n)|\text{vec}(\mathbf{\Phi}_c{}^n)) \geq F(\text{vec}(\mathbf{\Phi}_c{}^n)|\text{vec}(\mathbf{\Phi}_c{}^{n-1}))$.

Appendix C
Proof of proposition 2

Problem (P1.4) is a sub-optimization of (P1.5). Therefore, the optimal objective value of problem (P1.4) is not higher than that of (P1.5).

Suppose that $\hat{\mathbf{\Phi}}_c$ is a feasible solution to (P1.5), where $\hat{\mathbf{\Phi}}_c(i) < 1$. We can always find a solution $\hat{\mathbf{\Phi}}_c'$ achieving a better performance, which is defined as

$$\hat{\mathbf{\Phi}}_c'(j) = \begin{cases} \hat{\mathbf{\Phi}}_c(j), \text{for } \forall \ j \neq i \\ k\hat{\mathbf{\Phi}}_c(j), \ j = i \end{cases} \tag{47}$$

If $(\mathbf{a}(i)+\mathbf{b}(i))\hat{\mathbf{\Phi}}_c(i) > 0$, we set $k = 1/\hat{\mathbf{\Phi}}_c(i)$. Otherwise, we set $k = -1/\hat{\mathbf{\Phi}}_c(i)$. The difference between the performance of $\hat{\mathbf{\Phi}}_c'$ and that of $\hat{\mathbf{\Phi}}_c$ is derived as

$$\begin{aligned} &F(\hat{\mathbf{\Phi}}_c'|\mathbf{\Phi}_c^{n-1}) - F(\hat{\mathbf{\Phi}}_c'|\mathbf{\Phi}_c^{n-1}) \\ &= (k-1)(\mathbf{a}(i)+\mathbf{b}(i))\hat{\mathbf{\Phi}}_c(i) > 0. \end{aligned} \tag{48}$$

where $\mathbf{a} = \text{vec}(\mathbf{\Phi}_c{}^{n-1})\mathbf{\Theta}\mathbf{\Theta}^H$ and $\mathbf{b} = \mathbf{w}^*\mathbf{H}_d^H\mathbf{\Theta}$. Therefore, the optimal objective value of (P1.5) is not higher than that of (P1.4). The proof is completed.

References

[1] J. Hu, Q. Wang, and K. Yang, "Energy self-sustainability in full-spectrum 6g," *Accepted by IEEE Wireless Communications*, September 2020.

[2] H. J. Visser and R. J. M. Vullers, "RF Energy Harvesting and Transport for Wireless Sensor Network Applications: Principles and Requirements," *Proceedings of the IEEE*, vol. 101, no. 6, pp. 1410–1423, 2013.

[3] J. Hu, K. Yang, G. Wen, and L. Hanzo, "Integrated data and energy communication network: A comprehensive survey," *IEEE Communications Surveys Tutorials*, vol. 20, no. 4, pp. 3169–3219, 2018.

[4] J. Zheng, Y. Cai, X. Shen, Z. Zheng, and W. Yang, "Green energy optimization in energy harvesting wireless sensor networks," *IEEE Communications Magazine*, vol. 53, no. 11, pp. 150–157, 2015.

[5] B. Clerckx and E. Bayguzina, "Low-complexity adaptive multisine waveform design for wireless power transfer," *IEEE Antennas and Wireless Propagation Letters*, vol. 16, pp. 2207–2210, 2017.

[6] B. Clerckx, "Wireless information and power transfer: Nonlinearity, waveform design, and rate-energy tradeoff," *IEEE Transactions on Signal Processing*, vol. 66, no. 4, pp. 847–862, 2018.

[7] B. Clerckx and E. Bayguzina, "Waveform design for wireless power transfer," *IEEE Transactions on Signal Processing*, vol. 64, no. 23, pp. 6313–6328, 2016.

[8] Y. Huang and B. Clerckx, "Waveform design for wireless power transfer with limited feedback," *IEEE Transactions on Wireless Communications*, vol. 17, no. 1, pp. 415–429, 2018.

[9] R. Zhang and C. K. Ho, "MIMO Broadcasting for Simultaneous Wireless Information and Power Transfer," *IEEE Transactions on Wireless Communications*, vol. 12, no. 5, pp. 1989–2001, 2013.

[10] S. Zhong and X. Wang, "Wireless Power Transfer by Beamspace Large-Scale MIMO With Lens Antenna Array," *IEEE Transactions on Wireless Communications*, vol. 18, no. 2, pp. 1390–1403, 2019.

[11] X. Chen, H. V. Cheng, A. Liu, K. Shen, and M.-J. Zhao, "Mixed-timescale beamforming and power splitting for massive mimo aided swipt iot network," *IEEE Wireless Communications Letters*, vol. 9, no. 1, pp. 78–82, 2020.

[12] Z. Zhu, N. Wang, W. Hao, Z. Wang, and I. Lee, "Robust beamforming designs in secure mimo swipt iot networks with a nonlinear channel model," *IEEE Internet of Things Journal*, vol. 8, no. 3, pp. 1702–1715, 2021.

[13] J. Zhang, G. Zheng, I. Krikidis, and R. Zhang, "Fast specific absorption rate aware beamforming for downlink swipt via deep learning," *IEEE Transactions on Vehicular Technology*, vol. 69, no. 12, pp. 16178–16182, 2020.

[14] G. Dong, H. Zhang, and D. Yuan, "Downlink achievable rate of massive mimo enabled swipt systems over rician channels," *IEEE Communications Letters*, vol. 22, no. 3, pp. 578–581, 2018.

[15] C. Song and Y. Jeon, "Weighted mmse precoder designs for sum-utility maximization in multi-user swipt network-mimo with per-bs power constraints," *IEEE Transactions on Vehicular Technology*, vol. 67, no. 3, pp. 2809–2813, 2018.

[16] T. J. Cui, M. Q. Qi, X. Wan, J. Zhao, and Q. Cheng, "Coding metamaterials, digital metamaterials and programmable metamaterials," *Light Science & Applications*, vol. 3, no. 10, p. e218, 2014.

[17] S. Hong, C. Pan, H. Ren, K. Wang, and A. Nallanathan, "Artificial-noise-aided secure mimo wireless communications via intelligent reflecting surface," *IEEE Transactions on Communications*, vol. 68, no. 12, pp. 7851–7866, 2020.

[18] O. T. Demir and E. Björnson, "Joint power control and lsfd for wireless-powered cell-free massive mimo," *IEEE Transactions on Wireless Communications*, vol. 20, no. 3, pp. 1756–1769, 2021.

[19] M. D. Renzo, M. Debbah, and D. P. *et al*, "Smart Radio Environments Empowered by Reconfigurable AI Meta-Surfaces: an Idea Whose Time Has Come," *EURASIP J. Wireless Commun. Networking*, vol. 2019, no. 1, p. 129, 2019.

[20] Q. Wu and R. Zhang, "Towards Smart and Reconfigurable Environment: Intelligent Reflecting Surface Aided Wireless Network," *IEEE Communications Magazine*, vol. 58, no. 1, pp. 106–112, 2020.

[21] J. Zhang, E. Bjőrnson, M. Matthaiou, D. W. K. Ng, H. Yang, and D. J. Love, "Prospective Multiple Antenna Technologies for Beyond 5G," *IEEE Journal on Selected Areas in Communications*, pp. 1–1, 2020.

[22] C. Pan, H. Ren, K. Wang, J. F. Kolb, M. Elkashlan, M. Chen, M. Di Renzo, Y. Hao, J. Wang, A. L. Swindlehurst, X. You, and L. Hanzo, "Reconfigurable intelligent surfaces for 6g systems: Principles, applications, and research directions," *IEEE Communications Magazine*, vol. 59, no. 6, pp. 14–20, 2021.

[23] M. Hua, L. Yang, Q. Wu, C. Pan, C. Li, and A. Lee Swindlehurst, "Uav-assisted intelligent reflecting surface symbiotic radio system," *IEEE Transactions on Wireless Communications*, pp. 1–1, 2021.

[24] Q. Wu and R. Zhang, "Joint active and passive beamforming optimization for intelligent reflecting surface assisted swipt under qos constraints," *IEEE Journal on Selected Areas in Communications*, vol. 38, no. 8, pp. 1735–1748, 2020.

[25] F. E. Bouanani, S. Muhaidat, P. C. Sofotasios, O. A. Dobre, and O. S. Badarneh, "Performance analysis of intelligent reflecting surface aided wireless networks with wireless power transfer," *IEEE Communications Letters*, vol. 25, no. 3, pp. 793–797, 2021.

[26] Y. Zheng, S. Bi, Y. J. Zhang, Z. Quan, and H. Wang, "Intelligent reflecting surface enhanced user cooperation in wireless powered communication networks," *IEEE Wireless Communications Letters*, vol. 9, no. 6, pp. 901–905, 2020.

[27] C. Pan, H. Ren, K. Wang, M. Elkashlan, A. Nallanathan, J. Wang, and L. Hanzo, "Intelligent reflecting surface aided mimo broadcasting for simultaneous wireless information and power transfer," *IEEE Journal on Selected Areas in Communications*, vol. 38, no. 8, pp. 1719–1734, 2020.

[28] Y. Zou, S. Gong, J. Xu, W. Cheng, D. T. Hoang, and D. Niyato, "Wireless powered intelligent reflecting surfaces for enhancing wireless communications," *IEEE Transactions on Vehicular Technology*, vol. 69, no. 10, pp. 12369–12373, 2020.

[29] B. Lyu, P. Ramezani, D. T. Hoang, S. Gong, Z. Yang, and A. Jamalipour, "Optimized energy and information relaying in self-sustainable irs-empowered wpcn," *IEEE Transactions on Communications*, vol. 69, no. 1, pp. 619–633, 2021.

[30] N. Hehao and L. Ni, "Intelligent reflect surface aided secure transmission in mimo channel with swipt," *IEEE Access*, vol. 8, pp. 192132–192140, 2020.

[31] Q. Wu and R. Zhang, "Weighted sum power maximization for intelligent reflecting surface aided swipt," *IEEE Wireless Communications Letters*, vol. 9, no. 5, pp. 586–590, 2020.

[32] W. Yan, X. Yuan, Z.-Q. He, and X. Kuai, "Passive beamforming and information transfer design for reconfigurable intelligent surfaces aided multiuser mimo systems," *IEEE Journal on Selected Areas in Communications*, vol. 38, no. 8, pp. 1793–1808, 2020.

[33] E. Boshkovska, D. W. K. Ng, N. Zlatanov, and R. Schober, "Practical Non-Linear Energy Harvesting Model and Resource Allocation for SWIPT Systems," *IEEE Communications Letters*, vol. 19, no. 12, pp. 2082–2085, 2015.

[34] Y. Lu, K. Xiong, P. Fan, Z. Ding, Z. Zhong, and K. B. Letaief, "Global energy efficiency in secure miso swipt systems with non-linear power-splitting eh model," *IEEE Journal on Selected Areas in Communications*, vol. 37, no. 1, pp. 216–232, 2019.